AD

AD-E404 228

Technical Report ARMET-TR-19004

ANALYSIS OF COLLECTED SEMI-ACTIVE LASER (SAL) IMAGES

Zaw T. Han
João M. Romano
Luz Florez Manduca

August 2020

U.S. ARMY COMBAT CAPABILITIES DEVELOPMENT
COMMAND ARMAMENTS CENTER

Munitions Engineering Technology Center

Picatinny Arsenal, New Jersey

The views, opinions, and/or findings contained in this report are those of the author(s) and should not be construed as an official Department of the Army position, policy, or decision, unless so designated by other documentation.

The citation in this report of the names of commercial firms or commercially available products or services does not constitute official endorsement by or approval of the U.S. Government.

Destroy by any means possible to prevent disclosure of contents or reconstruction of the document. Do not return to the originator.

.

REPORT DOCUMENTATION PAGE

Form Approved
OMB No. 0704-01-0188

1. REPORT DATE (DD-MM-YYYY)	2. REPORT TYPE	3. DATES COVERED (*From - To*)
August 2020	Final	

4. TITLE AND SUBTITLE

Analysis of Collected Semi-Active Laser (SAL) Images

5a. CONTRACT NUMBER

5b. GRANT NUMBER

5c. PROGRAM ELEMENT NUMBER

6. AUTHORS

Zaw T. Han, João M. Romano, and Luz Florez Manduca

5d. PROJECT NUMBER

5e. TASK NUMBER

5f. WORK UNIT NUMBER

7. PERFORMING ORGANIZATION NAME(S) AND ADDRESS(ES)
U.S. Army CCDC AC, METC
Fuze & Precision Armaments Directorate
(FCDD-ACM-FP)
Picatinny Arsenal, NJ 07806-5000

8. PERFORMING ORGANIZATION REPORT NUMBER

9. SPONSORING/MONITORING AGENCY NAME(S) AND ADDRESS(ES)
U.S. Army CCDC AC, ESIC
Knowledge & Process Management Office (FCDD-ACE-K)
Picatinny Arsenal, NJ 07806-5000

10. SPONSOR/MONITOR'S ACRONYM(S)

11. SPONSOR/MONITOR'S REPORT NUMBER(S)
Technical Report ARMET-TR-19004

12. DISTRIBUTION/AVAILABILITY STATEMENT
Approved for public release; distribution is unlimited.

13. SUPPLEMENTARY NOTES

14. ABSTRACT

This paper discusses the use of EO imagery as a means to detect a SAL signal in a natural cluttered background. The paper discusses the method by which one can detect and extrapolate the SAL signal from clutter by subtracting two images where the requirement is that one of the two images contains the SAL signal, but not both. The images were collected at the U.S. Army Combat Capabilities Development Command Armaments Center, Picatinny Arsenal, NJ, using an E2V complementary metal-oxide-semiconductor (CMOS) camera at different integration times using various bandpass and highpass filters. For this report, the ability to discriminate a SAL signal from natural clutter background for images collected with an integration time of 25 μs for the highpass filter and integration times of 0.3 and 5 ms for the bandpass filter is examined. Sensitivity analysis are presented in this study using PDF curves that clearly demonstrate the ability to detect SAL signals from the natural cluttered scene. An assessment between highpass and bandpass filters with the respective different integration times as well as a description of the pros and cons for each filter can be also found in the report.

15. SUBJECT TERMS
Bandpass Highpass Integration time Misaligned Semi-Active Laser (SAL) Electro-Optical (EO) Probability Density Function (PDF) Complementary Metal-Oxide-Semiconductor (CMOS)

16. SECURITY CLASSIFICATION OF:			17. LIMITATION OF ABSTRACT	18. NUMBER OF PAGES	19a. NAME OF RESPONSIBLE PERSON
a. REPORT	b. ABSTRACT	c. THIS PAGE			Zaw T. Han
U	U	U	SAR	29	19b. TELEPHONE NUMBER (Include area code) (973) 724-5356

Standard Form 298 (Rev. 8/98)
Prescribed by ANSI Std. Z39.1

CONTENTS

FIGURES

FIGURES
(continued)

INTRODUCTION

Semi-active laser (SAL) seekers are a considerably cheap alternative for smart munitions in applications where (1) the Global Position System (GPS) is not available, (2) the target's GPS position is not available, (3) the target is moving, or (4) high precision is necessary to limit collateral damage. Current munition SAL seekers use, but are not limited to, a quad-cell (quadrant array) made of pin silicon photodiodes to detect and track SAL signals; however, there has been a change to move toward imagers, primarily Indium Gallium Arsenide (InGaAs), for SAL spot detection and tracking. Imagers bring several benefits such as: (1) multi-code spatial tracking; (2) better angle resolution for SAL tracking and navigation; and (3) multi-purpose imagers for target detection and tracking. However, InGaAs imagers are quite expensive when compared to a quad-cell seeker. For example, an InGaAs focal plane array (FPA) can potentially cost between $15,000 and $20,000, while a quad-cell seeker can cost approximately $5,000.

In this report, complementary metal-oxide-semiconductor (CMOS) imagers will be explored as a cheaper alternative to detect and track SAL signals in a natural cluttered background. Although the cost of CMOS imagers is very attractive, one concern over their use is that despite having good quantum efficiency (QE) values (around 400 and 900 μm), the QE drops very low (approximately a few %) at 1,064 μm. At 1,550 μm, eye-safe SAL designation, CMOS imagers cannot detect the SAL signal. On the other hand, InGaAs imagers are capable of detecting both the 1,064 and 1,550-μm signals. For this report, only the detection of 1,064-μm SAL signals will be focused on with the CMOS imager for different integration times and for various bandpass and highpass filters for registered and unregistered imagery. The idea is that CMOS cameras are extremely cheap sensors and that with the right filter and supporting algorithm/electronics such a payload could be implemented into small and cheap munitions.

An important topic not discussed in this report is the electronic and/or processing by which the subsystem ensures that it collects consecutive imagery with and without SAL signals. By collecting and processing (e.g., subtracting) two such images, one is able to increase the signal-to-clutter ratio (SCR) between the SAL signal and background clutter. However, as it will be shown, both the choice of integration times and filter used impact the SCR and the ability to detect the intended signal.

The concept of operations (CONOPS) for a munition with a SAL seeker is shown in figure 1, where a soldier designates (or illuminates) the desired objects using a designator (high energy laser emitter) with a specific code. The pulses are reflected from the target back to munition seeker (ref.1), and these pulses are then processed by the seeker sub-system to estimate the laser spot (on the target) position and maneuver the munition to hit the intended target (ref. 2).

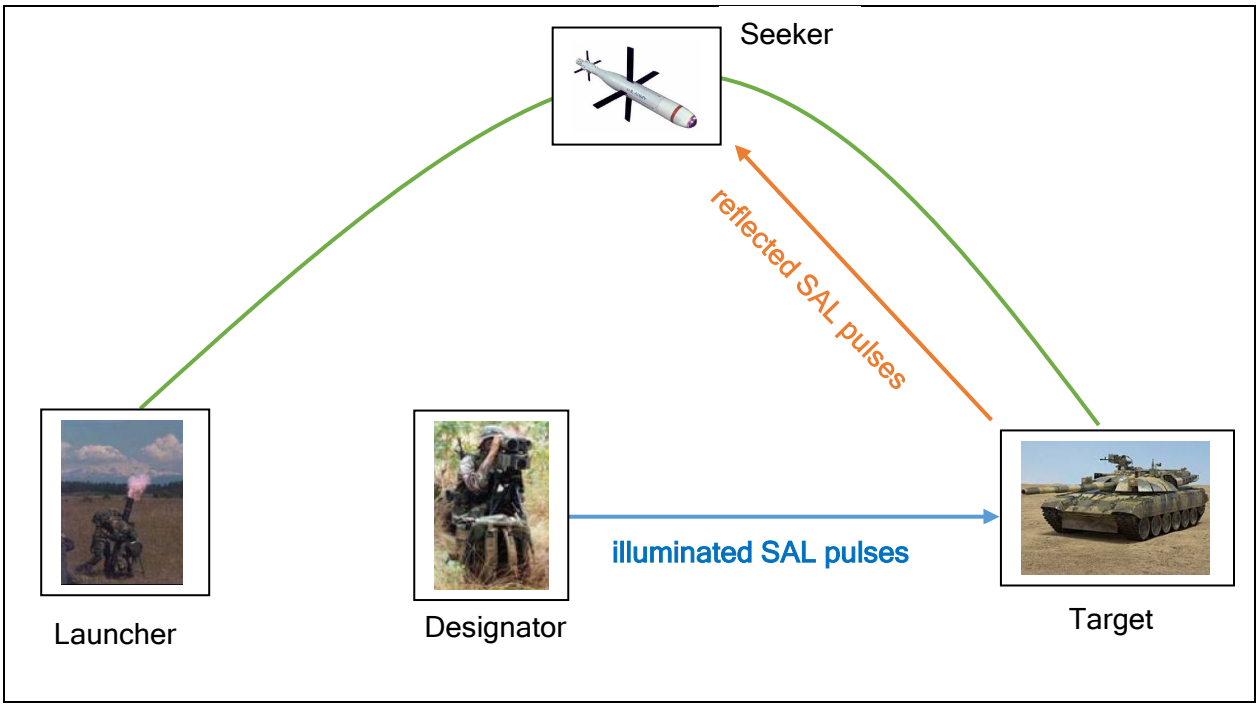

Figure 1
Operational overview of SAL seeker munition

This report focuses on demonstrating, through a variety of analyses, how a combination of integration and/or filter choice affects the performance of the system in detecting the SAL signal with an available commercially off-the-shelf CMOS camera.

DATA COLLECTION

Data Collection Description

The data were collected by E2V CMOS image sensor and compact folded resonator (CFR) pulse Neodymium-doped Yttrium Aluminum Garnet (Nd:YAG) laser. The basic setup for the tower is shown in figure 1.

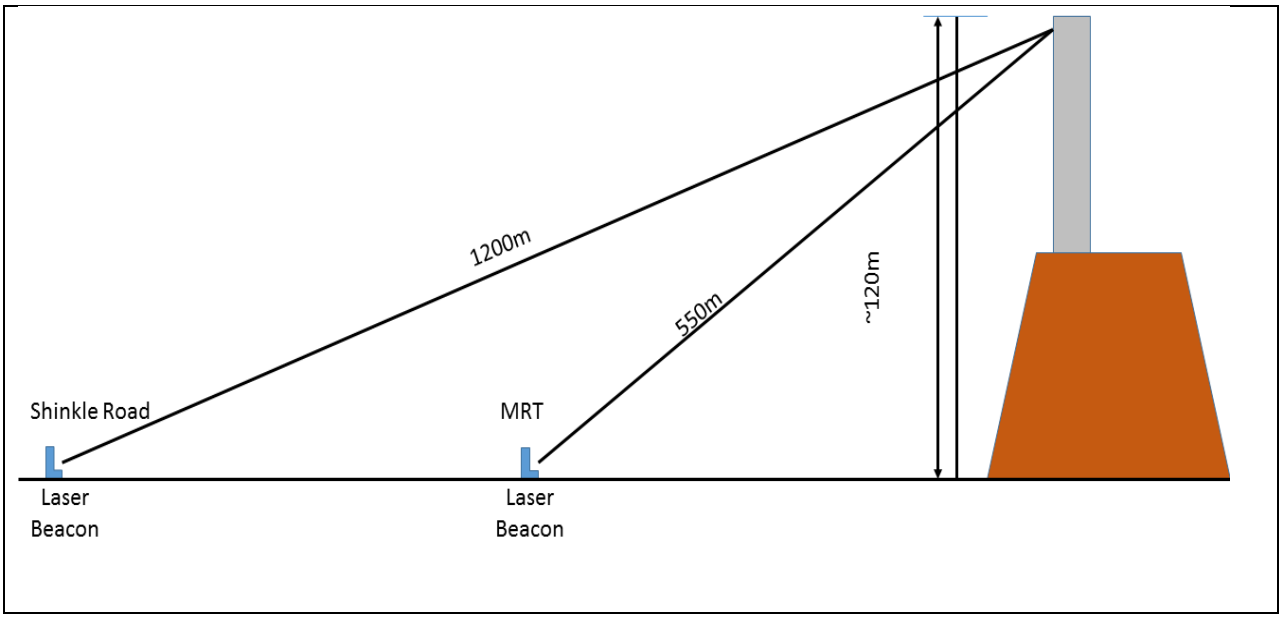

Note: The units under test (UUT) will be at the tower at a height of about 120 m from the ground. Two laser beacons will be placed in the mid-range and on Shinkle road.

Figure 2
Basic test setup

The laser source used for this data collection exercise was the laser beacon (LB). This LB was specifically designed for use in the "end-to-end" system demonstration test during the mid-range munition proof of principle demonstration phase. The UUT will be located on the 6th floor of the tower passively collecting imagery of the scene where the LB will be placed 550 m from the UUT field of view (FOV) as shown in figure 2. Figure 3 illustrates the topographic view of the data collection where the LB will be placed inside the mid-range test site (MRTS) around 550 m from the sensor.

Figure 3
Topographic view of the test

Figure 4 illustrates the setup at the MRTS (left) and at the tower (right) where a signal generator will be connected to the LB in order to generate a time coded pulse for the test. An area of with approximately a 6-m radius was marked as safety danger zone. At the tower, the E2V UUT cameras collected the data using specialized filters. Each camera was connected to a computer and the data stamped accordingly. Finally, each computer and the LB were connected to a GPS receiver in order to keep all machines synchronized. For LB specifications, see table 1.

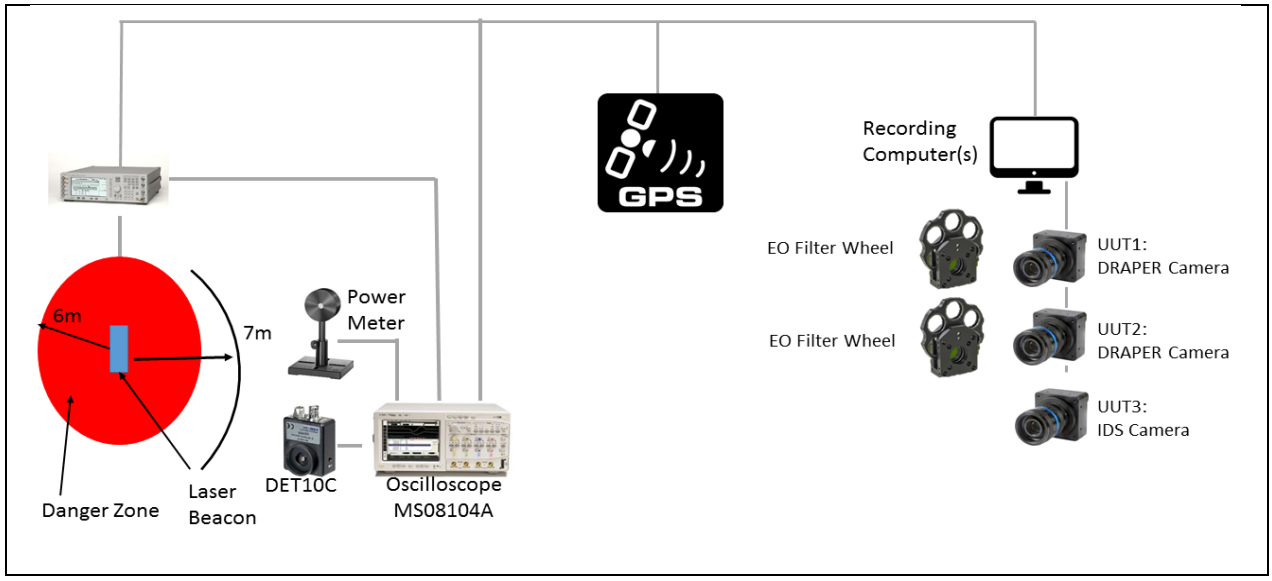

Note: The test will consist of three CMOS cameras at the tower connected to one or more recording computers.

Figure 4
Detailed site/tower test setup

Table 1
LB specifications

LB specifications	Parameter
Wavelength (λ)	1,064 μm
Nominal pulse width	20 ns
Pulse repetition frequency (PRF)	up to 20 Hz
Maximum pulse energy from laser	140 mJ
Energy drift over 8 hr	<10%
Flash lamp lifetime	>20 million shots
Target reflectance	0.5

Cameras and Specifications

The CMOS camera used for this data collection was the E2V CMOS near infrared (NIR)-enhanced ruby 1.3 M pixels EV76C661, with an FPA of 1280 x 1024 pixels, 1/1.8-in. format, and front-illumination. A five transistors (5T) square pixels design provides both electronic rolling shutter (ERS) and global shutter (GS) capability at a reduced read noise of 24$\bar{e}$. Table 2 presents the characteristics of the E2V CMOS camera.

Table 2
CMOS sensor parameter summary

SENSOR CHARACTERISTICS	E2V EV76C661
Resolution	1280 (H) x 1024 (V) pixels
Frame rate	60 fps
Minimum integration time	8 us (fractional integration time)
Shutter	GS or ERS
Temporal noise/read noise	ERS 6$\bar{e}$ GS 24$\bar{e}$
Technology	5T (effect QE)
Pixel size square	5.3 um
Objective lens	8 mm f/2
Micro-lens	yes (effect QE)
Optical format	(1/1.8) in.
Bit depth	10 bits
Front Side Illumination (FSI)	Front side illumination (FSI) (effect QE)
Dynamic range	60 dB (ERS)
QE	65% (peak); 3-4% at 1,060 nm
Dark signal	38 LSB_{10}/s (at 25 °C)
Well capacity	8400 $\bar{e}$
Conversion gain	8.5 $\bar{e}$/DN
Minimum integration	4 us
Starlight performance	50 mLux at 20 fps

For this test, the 2V sensor was operated in GS mode at 20 fps. The lens used for this test was the VX120 charge-coupled device (CCD)/CMOS lens from Universe Optics with a 12-mm focal lens, 12-mm aperture, with an FOV of 30.9-deg vertical FOV, 40.6-deg horizontal FOV, and 49.8-deg display FOV.

Semi-Active Laser (SAL) Simulator

The SAL simulator, or SAL Beacon (SB), simulates a 20-ns laser pulse that is similar to what is transmitted from a fielded designator for a given PRF. The SB uses a Quantel Big Sky CFR200 Compact Flash-lamp Pumped Q-switched Nd:YAG Laser operated at an energy level of 20 mJ, with each pulse having a pulsewidth of 20 ns reflected from the target plate of the LB as shown in figure 2. The sensor was positioned at the top of the Precision Armaments Laboratory (PAL) tower at a slanted range of 550 m and oriented in the direction of the target plate at an angle of 12.6 deg with respect to the normal to the reflected surface (i.e., target plate). The diffused and reflected laser pulses were collected by a CMOS lens with effective aperture of 12 mm. During the test, the weather was clear, and it was a sunny day with an optimal visibility of 20 km. All data was collected during the daytime. The laser was externally triggered at 20 Hz to synchronize the sensor to the laser pulse via GPS. The sensor was operated in GS mode, 20 fps, and 10-bit resolution. The data collection

consisted of a series of images for different sensor integration times for each of the four interference filters in addition to a set where no filter was used.

Data Products

The data consists of images collected by the E2V where the content of each image can be SAL with clutter or clutter only imagery. Figure 5 represents the type of imagery that was collected by the CMOS sensor. For this example, a highpass filter was used for 25-µs integration time for the CMOS sensor.

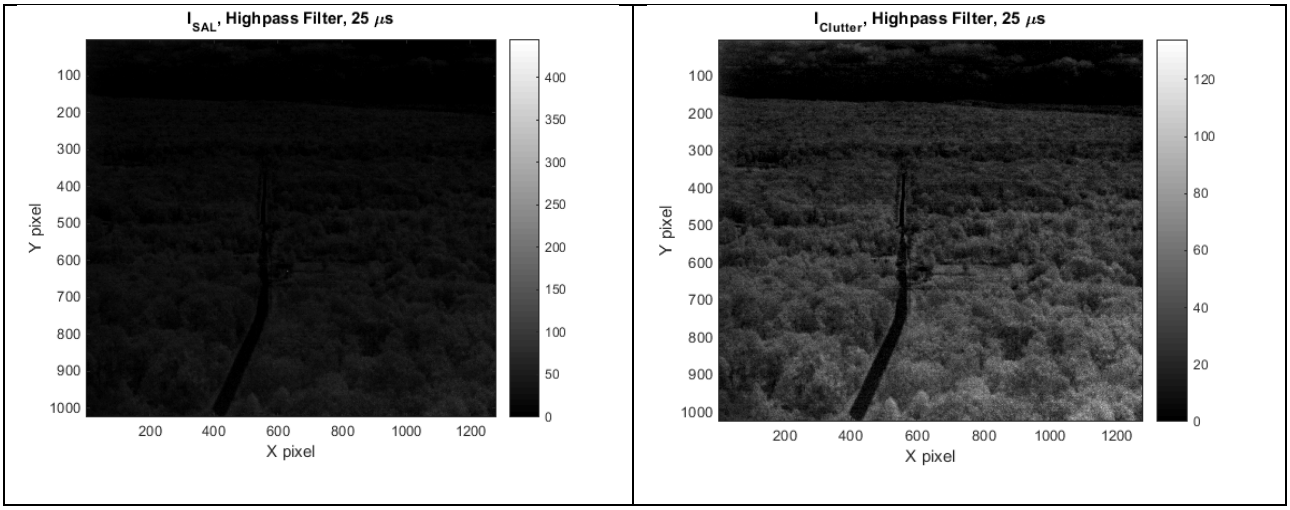

Note: (a) illustrates SAL signal embedded in clutter while (b) illustrates clutter only image.

(a) (b)

Figure 5
Data products collected by CMOS sensor

IMAGE ANALYSIS PROCEDURES

The seeker subsystem needs to be capable of collecting two consecutive images where one has the SAL signal embedded in the clutter, and the other only captures the clutter (no SAL signal). By doing so, and assuming that both images are collected together within a very small time period of each other, one can subtract both images in order to increase the SCR between the SAL signal and the background clutter, as shown in figures 6 through 8.

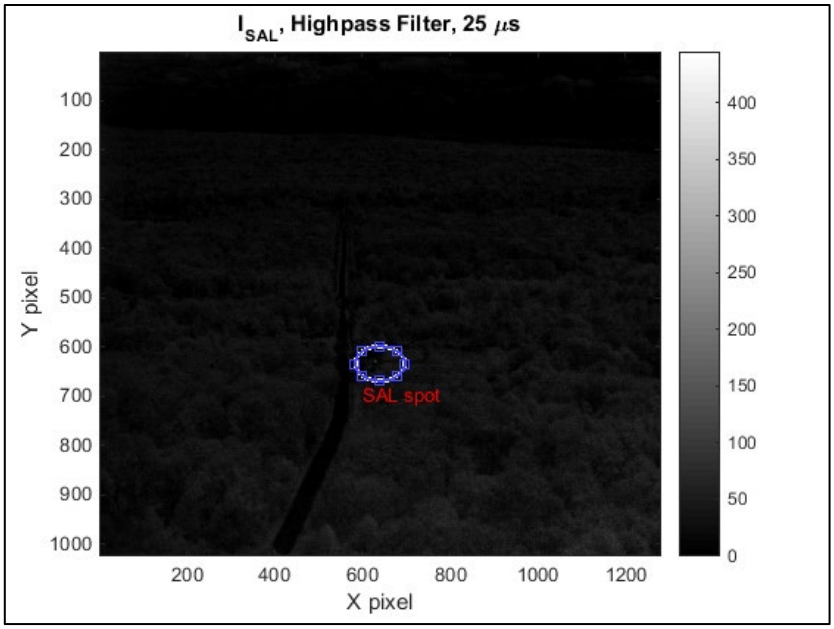

Figure 6
SAL image

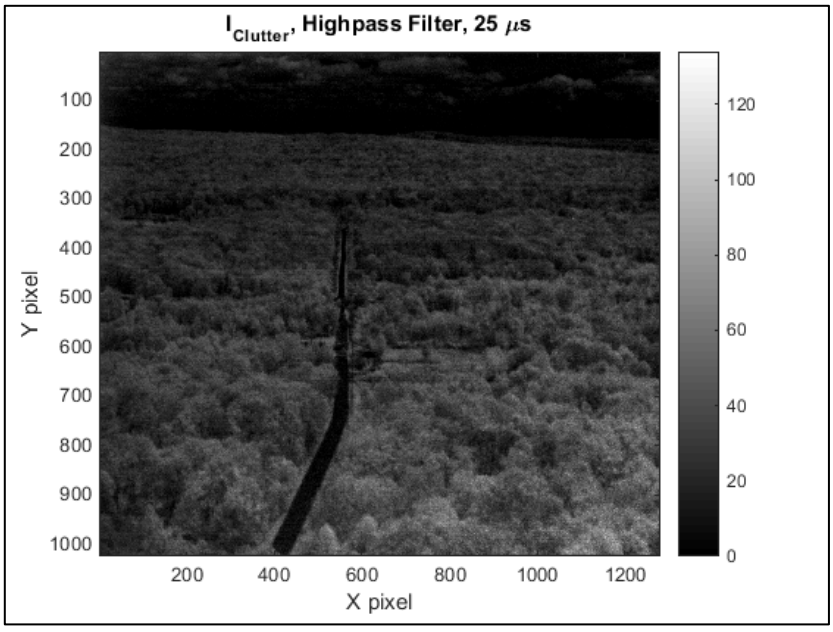

Figure 7
Clutter image

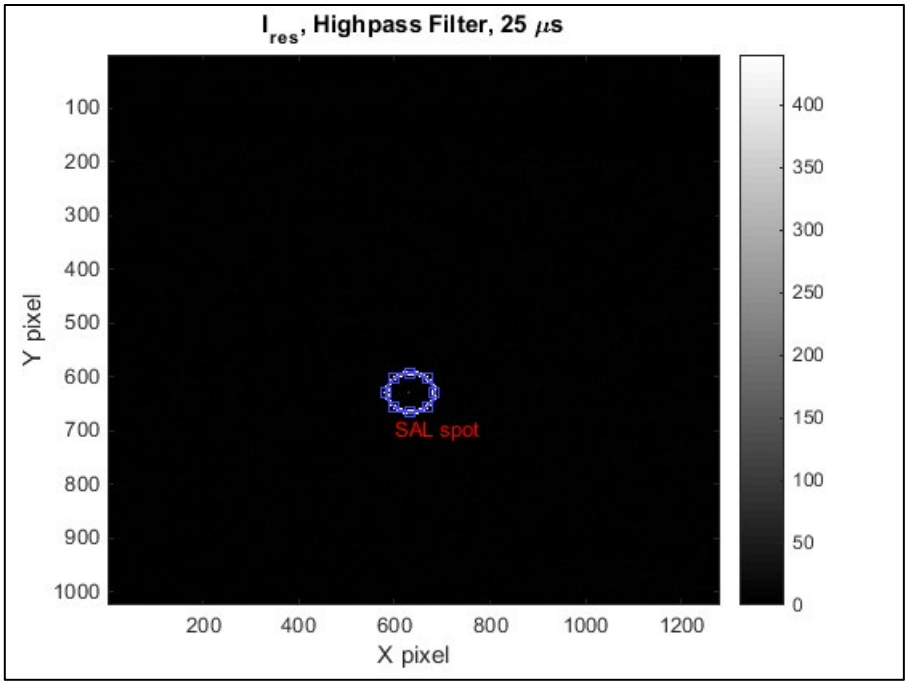

Figure 8
Residual image

In figures 6 through 8, an image with a SAL signal is acquired, in this case the integration time was 25 μs with a highpass filter, followed by another image where the SAL signal is not present. At this time, since there is no camera movement, the subtraction of these two images yields a residual image that demonstrates very little in the way of false alarms. The processing of the data, is represented as follows:

I_{res} is defined as the residual image and is the result of the subtraction of the two images, one with the SAL signal (I_{SAL}) and one with only clutter ($I_{clutter}$). This is demonstrated in equation 1.

$$\boldsymbol{I_{res} = I_{SAL} - I_{clutter}} \tag{1}$$

The residual image is in terms of counts [based on the analog to digital (AD) conversion]; it has no statistical meaning for data analysis or to develop adaptive thresholds. As a result, I_{res} is normalized based on its own global statistics as in equation 2:

$$\boldsymbol{I_{norm} = \frac{(I_{res}(x,y) - \mu(I_{res}))}{\sigma(I_{res})}} \tag{2}$$

where $I_{res}(x, y)$ is the x-y pixel location in the I_{res} image, and $\mu(I_{res})$ and $\sigma(I_{res})$ are the global mean and standard deviation, respectively, of the I_{res} image. Finally, I_{norm} is defined as the normalized residual image.

Figure 9 demonstrates that images I_{res} and I_{norm} are similar to each other except for the fact that scale on I_{res} image is in terms of AD counts, and I_{norm} is in standard deviations. For example, the SAL signal in the I_{norm} image is above 100 σ from the mean value of the image. From a statistical point of view, assuming that the residual clutter fits a normal distribution, then 99.99% of the residual data fits within ±5 σ, and a signal higher than ±5 σ can be seen as the anomaly to distribution. In this case, the signal is always positive because the energy from the SAL beacon is higher than the background after the subtraction, so the threshold will always be positive.

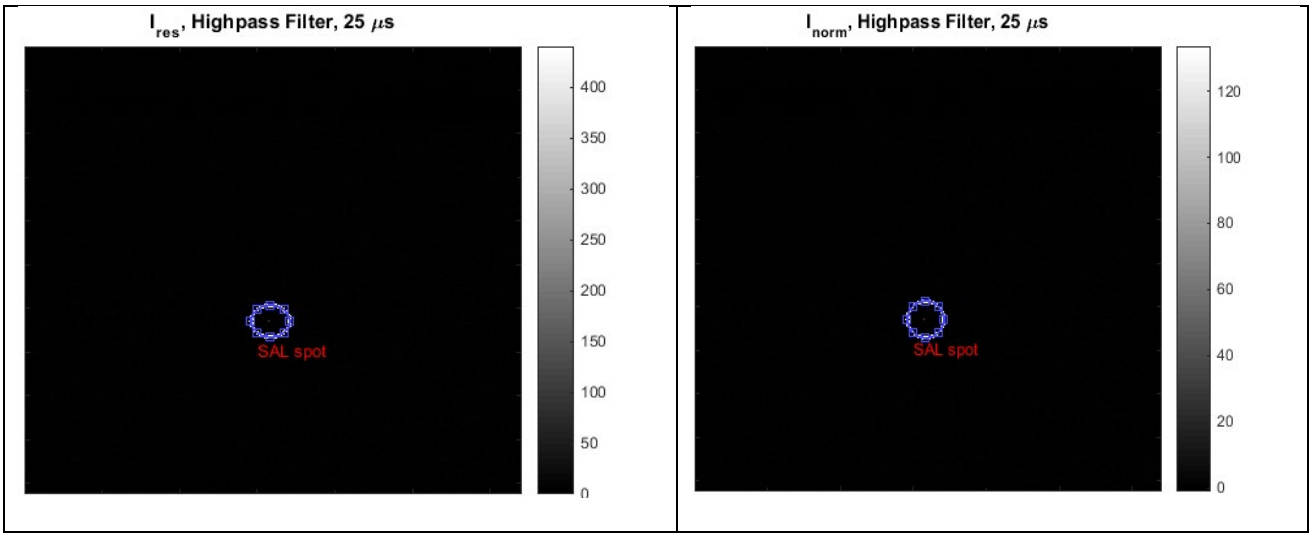

(a) (b)

Figure 9
The I_{res} and I_{norm} images for highpass filter with 25-μs integration time

Figure 10 illustrates the SAL signal strength in red and the clutter pixel maximum value in black. The mean clutter value is around zero due to equation 2. This figure compares the SAL signal strength to the background clutter over a number of consecutive images. The title at the top of the figure states that there are no misaligned pixels; as a result, it can be assumed that this would be the best case where the SCR between the SAL and clutter is maximum. It can also be assumed, as will be shown, that as the number of misaligned pixels between the I_{SAL} and $I_{clutter}$ increase, the residual image shows more artifacts due to the misalignment. As a result, these artifacts may have high σ values that are similar to the SAL signal strength, which results in false alarms.

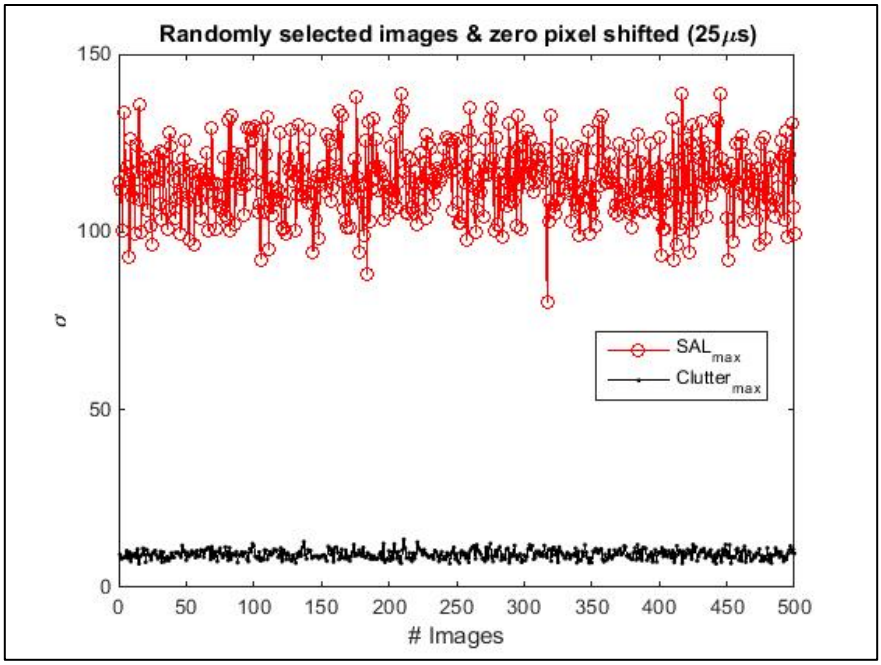

Figure 10
Highpass filter with 25-μs integration time SAL signal and maximum clutter values for 500 processed images with no misaligned pixels during the subtraction

Figure 11 illustrates a probability density function (PDF) analysis that will be used to compare the statistics of the clutter maximum values ($clutter_{max}$) and the SAL signal strength in σ over all of the images that were collected for a given filter and sensor integration time.

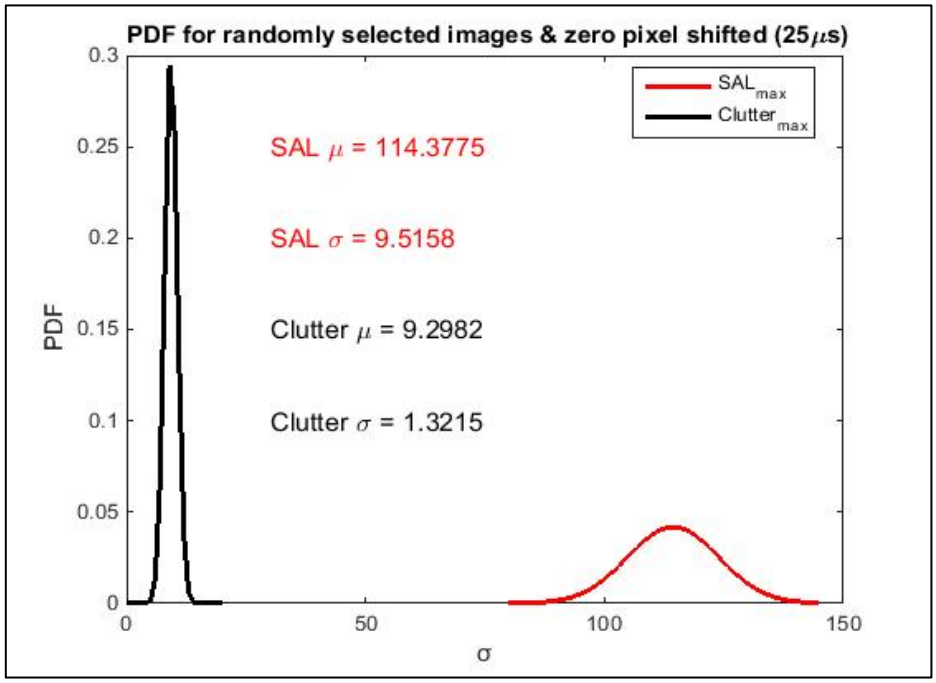

Figure 11
PDF for clutter and SAL signal for 500 processed images (highpass filter with 25-μs integration time) with no pixel misalignment

The main reason for showing the statistics of the maximum value of clutter is twofold: First, the background is composed of 99.99% of the pixels in the image, as a result, the statistic values such as mean and variance of the data when plotted into a normal distribution do not show anomalies (other than the SAL signal) that may exist in the image, because these anomalies are very few relative to the number of background pixels. Second, by looking at these clutter anomalies and plotting them as an entity of their own, the reader is able to visualize the strength of these anomalies with respect to the SAL signal. There is no need to plot the background clutter itself, because its statistics have shown to be around the 0 σ with a very tight distribution. Therefore, the $clutter_{max}$ is a more representative factor to false alarms.

Therefore, to calculate the PDF and assuming that the data fits a normal distribution, the mean (μ) and standard deviation (σ) are calculated for all the SAL and $clutter_{max}$ pixels. Those values are then used in equations 3 and 4 to yield the graph in figure 9.

$$PDF(SAL) = \frac{1}{\sigma(SAL)\sqrt{2\pi}} exp^{\left[-\frac{\left(SAL-\mu(SAL)\right)^2}{2\sigma(SAL)^2}\right]} \quad (3)$$

$$PDF(Clutter_{max}) = \frac{1}{\sigma(Clutter_{max})\sqrt{2\pi}} exp^{\left[-\frac{\left(Clutter_{max}-\mu(Clutter_{max})\right)^2}{2\sigma(Clutter_{max})^2}\right]} \quad (4)$$

As seen in figure 11, and by comparing to the results from figure 10, it can be clearly seen that the distribution fits the SAL signal well over the different images, where the signal strength mean value is around 114 σ, while the mean value for $clutter_{max}$ is around 9 σ.

In this particular case, it is clear that the $clutter_{max}$ strength values are extremely low compared to the SAL strength. Also, it is important to understand that for figure 11, only natural background clutter was taken into account for the PDF calculations. In fact, in the real data, a street light was present and it was labeled as man-made clutter. Further on, the impact of the street light in discriminating the SAL signal from the clutter (man-made and natural) will be shown.

Figure 11 also allows the user to understand the spread of these values through the different σ values. Although, in this particular case the reader does not see any overlap between SAL and $clutter_{max}$, later on when misregistration is purposely induced, it is important to understand when and how much these two signal statistics overlap.

Finally, in order to understand how the SAL signal strength compares in cases where image registration is not present or when it fails to register images successfully, misregistration errors of 1, 3, 5, 7, and 9 pixels offset in the ±x and ±y-axis were induced to understand how sensitive the signal strength is to misregistration when the $I_{clutter}$ and I_{SAL} images are subtracted.

RESULTS

This section will examine the SAL signal strength with respect to natural and man-made clutter as the integration times and changes to the filter types used vary. Furthermore, this section will evaluate the impact of misregistration errors on the signal strength when compared to clutter.

Bandpass Filter (center wavelength 1,075 nm, bandwidth 50 nm) with 5-ms Integration Time

This section examines the discrimination of a SAL signal from clutter for images that were collected using an integration time of 5 ms with a bandpass filter. Figure 12 illustrates the I_{SAL} and $I_{clutter}$ images collected from the sensor (i.e., unit under test). It is important to notice some key points that can be seen when comparing both images. First, the AD counts seen in the scale on the right of each image are very similar. This means that the effect of long exposure time, 5 ms, captured a significant amount of light from natural clutter in constrast to the SAL signal, which always is 20-ns wide.

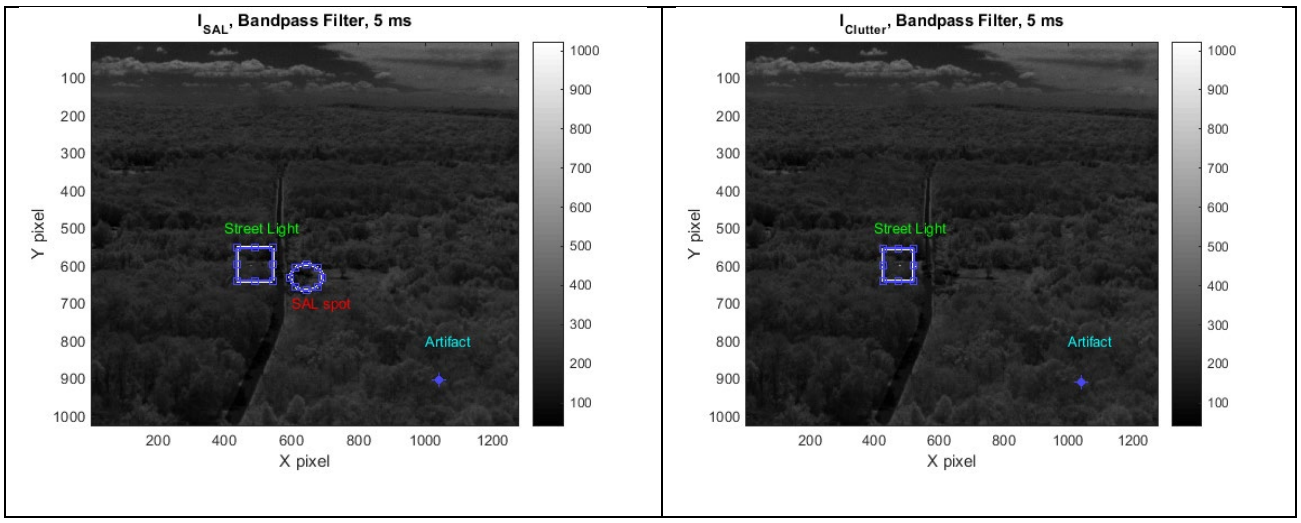

Note: The imagery was collected using a bandpass filter with a 5-ms integration time.

(a) (b)

Figure 12
Two images collected using the sensor where (a) shows the SAL spot image and the street light in natural clutter and (b) only shows natural clutter and the street light

As a result of this effect, caputring a image with a long integration time only affects the amount of light that one collects from the background scene and not the SAL signal. Second, the reader can observe that a street light is identified in the both scenes. The filter used in this experiment captures a sizable portion of the light spectrum, while at the same time, CMOS sensors have good sensitivity in this same region. On the other hand, CMOS sensors lack approximately 10% of the necessary sensitivity in the 1,064-nm region; this insinuates that the longer integration time collects light, more and more of the SAL signal will be embedded within the clutter to a point where it will become undetectable.

The following combinations show that a long integration time with bandpass filters are not suitable for SAL signal detection in the present state of man-made signals. Three factors affect the system's ability to detect the intended SAL signal:

1. Lack of sensitivity
2. Long integration
3. Short SAL pulse

Moreover, this sub-section will also evaluate the ability to discriminate the SAL signal when the light source is present and when it is not. Finally, the reader can also observe that an artifact is identified in both images in figure 12. This artifact is believed to be due to the camera itself and it is removed during post-processing, and thus is not evaluated.

Figure 13 illustrates the I_{norm} images after the I_{SAL} and $I_{clutter}$ images are subtracted from one another and then normalized in terms of standard deviations from the mean value of I_{res}. The main difference between figures 13a and b is that for image in figure 13a the street light is present, while in figure 13b the street light is removed so one can compare the effects of the light source present in a scene where a SAL signal needs to be detected.

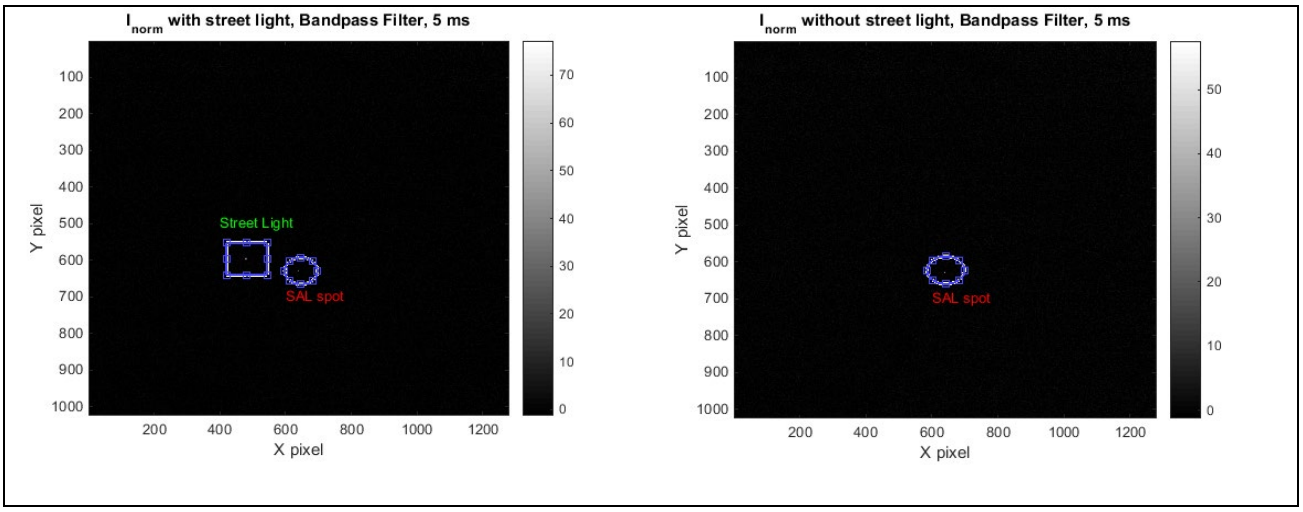

(a) (b)

Figure 13
(a) I_{norm} with street light signal (b) I_{norm} without street light signal for bandpass filter with 5 ms

Figure 14a illustrates the issue of man-made light sources in the scene versus no light sources in figure 14b. When the light source was present, more variability for the light was encountered for the following reason: when the street light was analyzed further, it was noticed that it only covered 1 pixel completely, while partially covering a second one. When collecting two images consecutively, it meant that, at times, the light source did not appear in the same pixel location every single time as a result of tower sway.

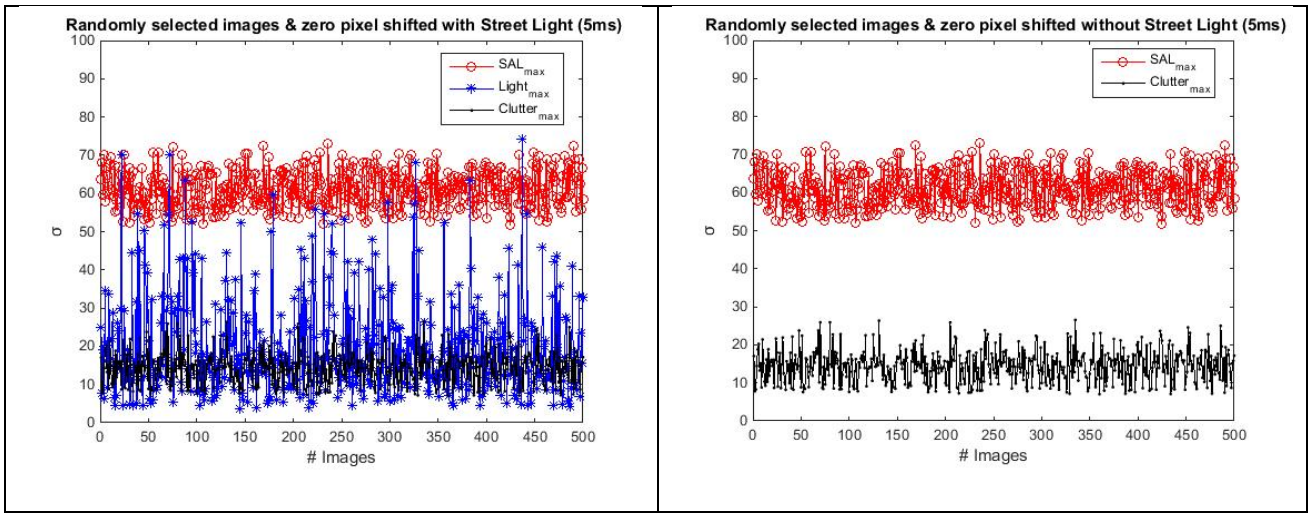

(a) (b)

Figure 14
SAL signal, maximum clutter and average clutter for 0-pixel misaligned images (a) with street light signal and (b) without street light signal by bandpass filter with 5-ms integration time

As a result, due to the subtraction, one could encounter a higher signal strength from the man-made light source when the pixels did not align and a weaker signal strength when they did. Consequently, one can see that the light source varies from very low σ values to, at times, higher values than the SAL signal itself as seen in image in figure 14a for data points 22, 72, 327, and 437. In comparison, such does not happen when the light source is not present in figure 14b where the SAL signal strength is always much higher than the maximum values seen from clutter for each of the analyzed imagery.

Figure 15 illustrates the effects of misregistration in the I_{norm} imagery for the detection of the SAL signal where figure 15a is the baseline at which the image was taken as is from the sensor, and figures 15b, c, and d are the result of misregistered SAL images and the maximum clutter values for 1, 5, and 9 misregistration pixels. As seen in figure 15, as the number of misregistered pixels increases, the street light energy surpasses the SAL signal energy, which increases the number of false alarms. As the number reaches up to 9 misregistered pixels, the SAL signal energy hovers around the clutter_{max} energy. As a result, when artificial light is present, it is important to keep images registered to limit the number of false alarms that may occur due to misregistrations. The reason for this is that the SAL pulse is 20 ns long, and, as a result, continuous light emissions are stronger than the SAL signal when they are misregistered from themselves.

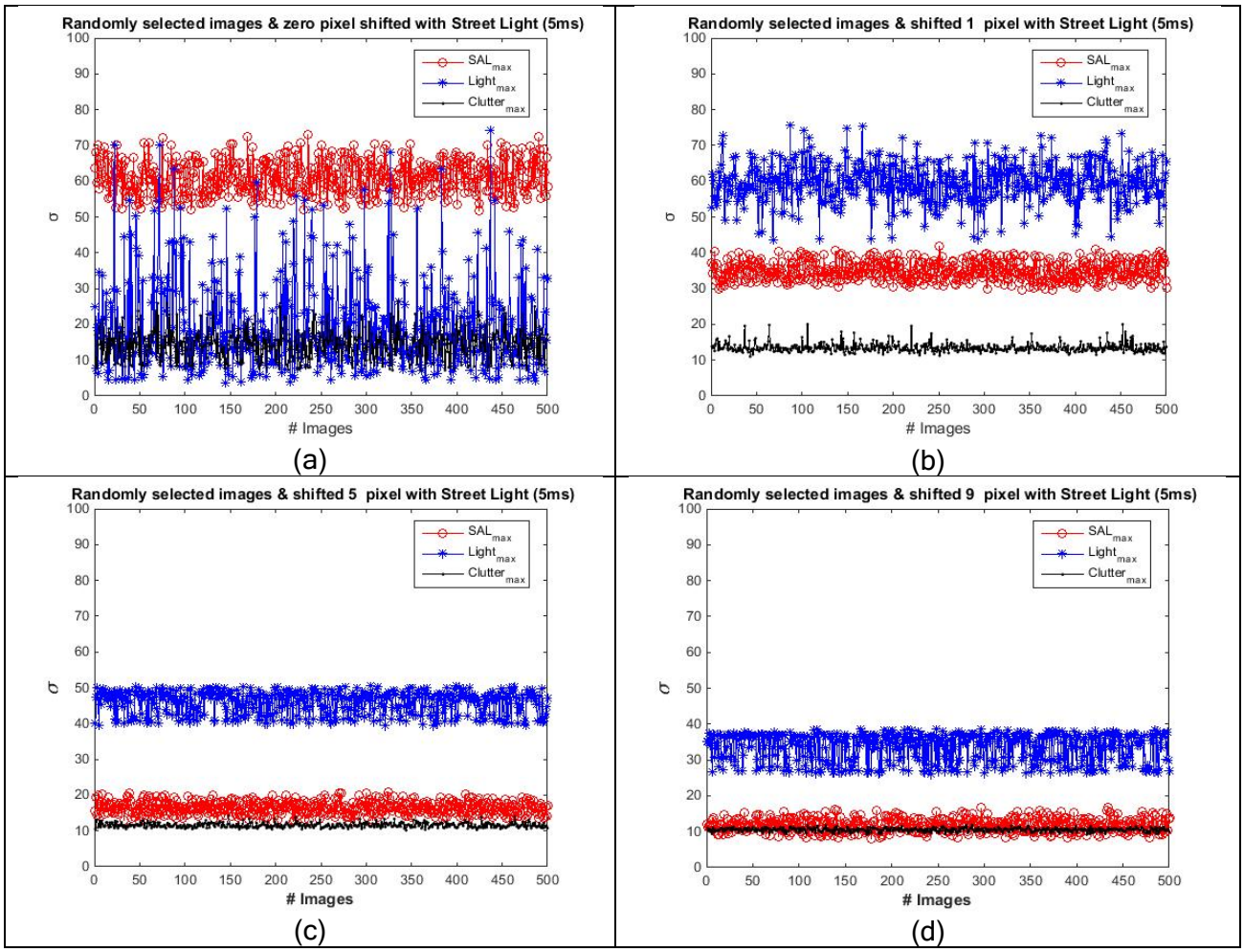

Note: As the number of misregistration pixels increases, the SAL signal energy decreases substantially. The street light on the other hand increases as it moves 1 pixel randomly; however, that energy also subsides as the number of unregistered pixels increases. On the other hand, background clutter stays mostly flat.

Figure 15
Illustration of misregistration effects onto SAL, street light, and $clutter_{max}$ energy

Figure 16 illustrates the PDF curves for the data shown in figure 15. As the number of misregistered pixels increases, one can observe the SAL signal distribution moving ever closer to the clutter distribution to the point that at 9 misregistered pixels the SAL signal is within the clutter distribution. On the other hand, with only one pixel misregistration, the man-made light source energy far exceeds the SAL signal's energy. One of the main reasons that this happens is that the SAL is 20 ns long, while the man-made light source is continuous. As a result, and as explained previously, since the integration time is 5 ms, the sensor continuously captures the emitted light, while the SAL signal is 20 ns, which is 1/250,000 of the 5 ms. Therefore, as the number of misregistered pixels increases, the light source energy becomes more pronounced compared to the SAL energy.

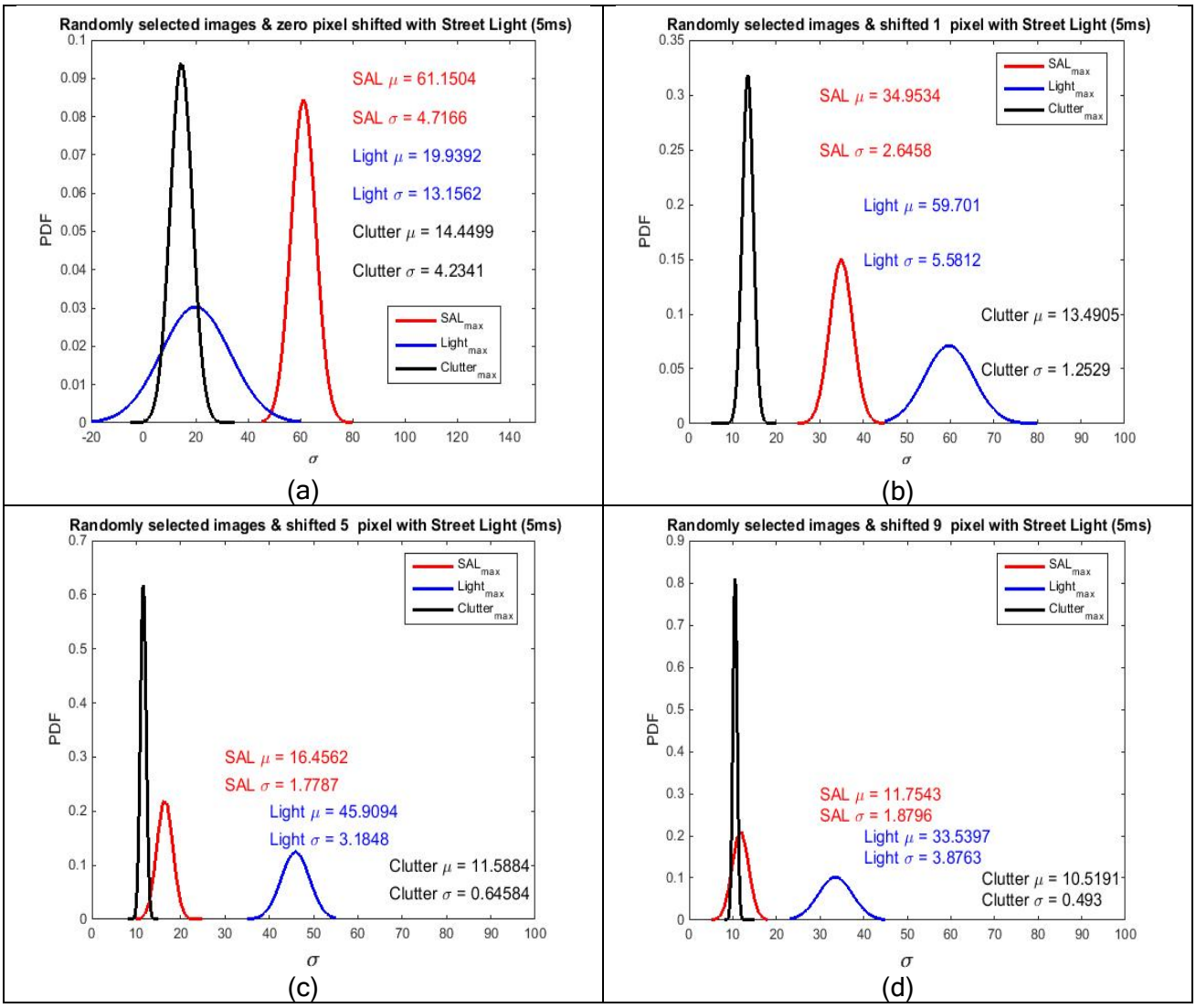

Figure 16
PDF curves for SAL, man-made light source, and clutter for 0, 1, 5, and 9 misregistration pixels

Bandpass Filter (center wavelength 1,075 nm, bandwidth 50 nm) with 0.3-ms Integration Time

This section will analyze the effects of shortening the integration time by a factor of a little more than 10 (5 to 0.3 ms) while using the same bandpass filter. For this specific case, the man-made light source was turned off, and, as a result, there will be no analysis comparing the effects of the light source for a shorter integration time.

Figure 17 illustrates the residual images that contain the SAL signal (fig.17a) and clutter only (fig.17b). Comparing the two images, one can observe that the SAL signal is quite above the clutter noise (>600σ) as shown in figure 17.

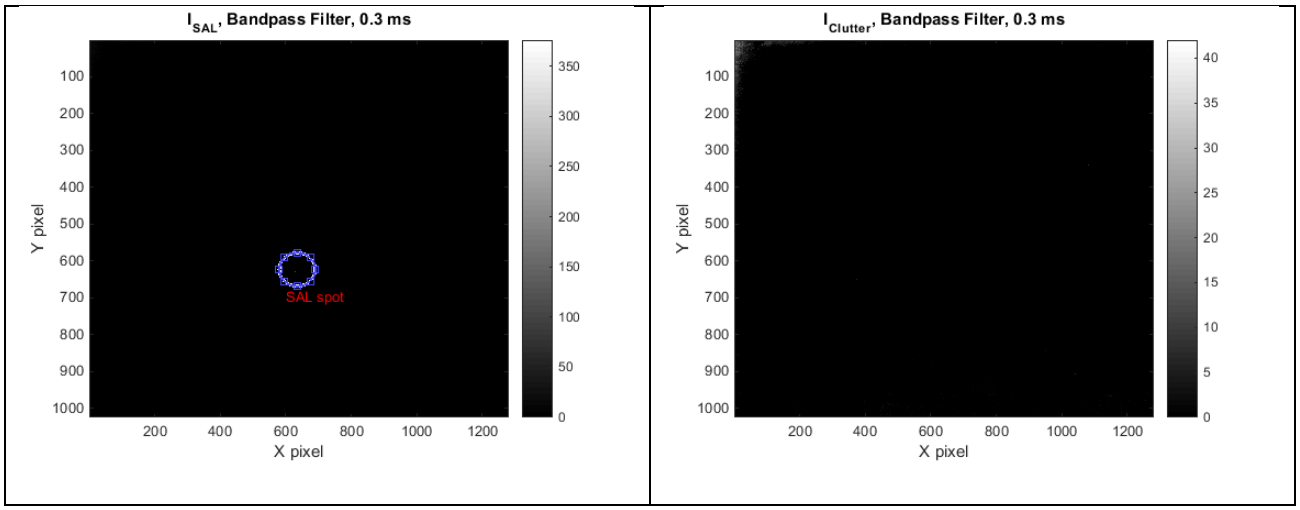

Note: As observed from both images, the SAL signal energy is considerably higher than natural clutter.

(a) (b)

Figure 17
(a) SAL spot image and (b) background clutter for 0.3-ms integration time with bandpass filter

Figure 18 illustrates the difference between SAL energy and background clutter as the number of misregistered pixels increases from 0 to 9. As it is shown, by reducing the integration time, which in turn reduces significantly the amount of background light captured by the sensor than in the previous sub-section, it increases the gap between the clutter and SAL signal to the point that, even with 9 misregistered pixels, the SAL signal is well above the clutter energy.

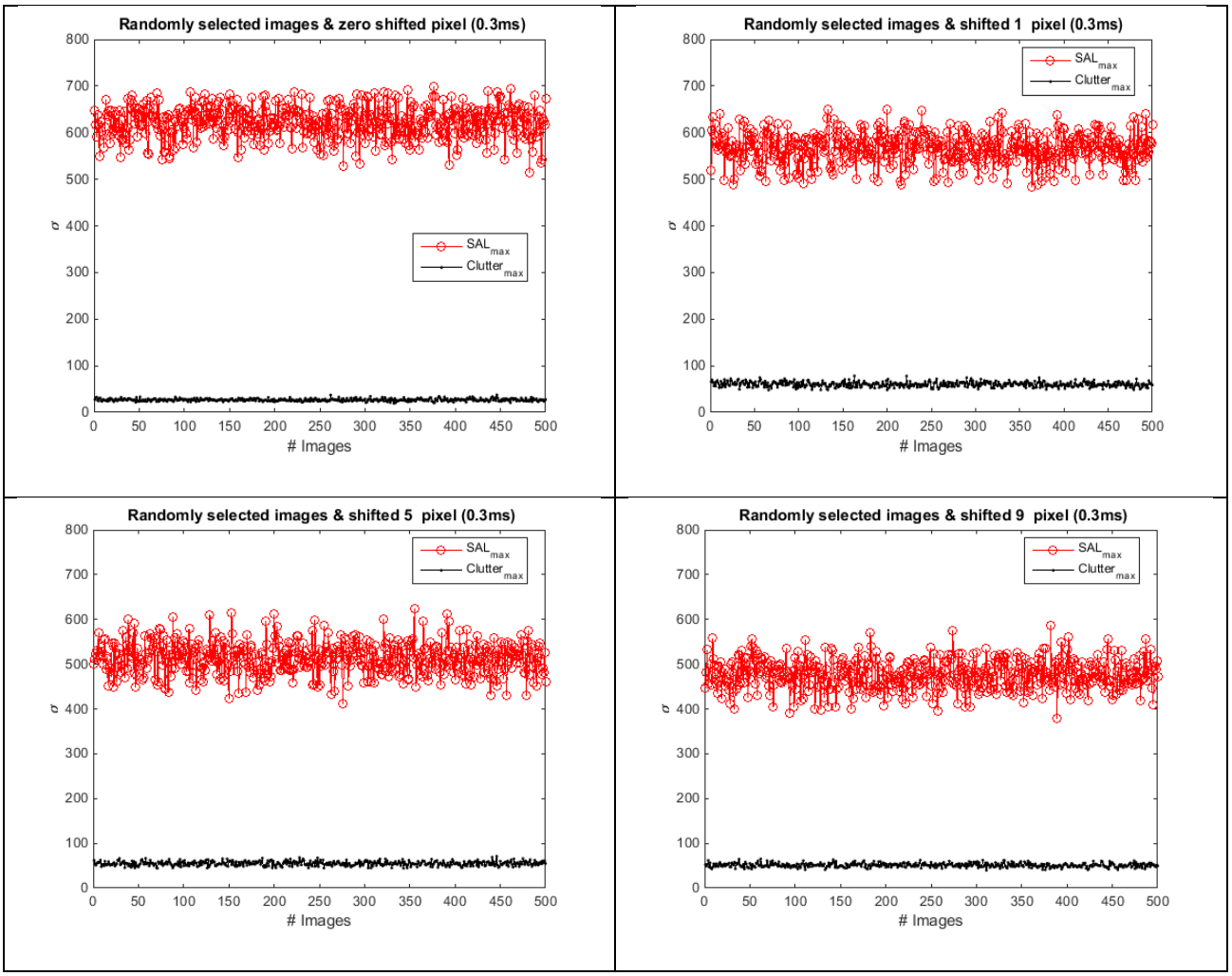

Note: The SAL signal energy is considerably higher than the clutter regardless of the number of misregistered pixels.

Figure 18
SAL and clutter energy comparison for 0, 1, 5, and 9 misregistered pixels for 0.3-ms integration time

Finally, figure 19 illustrates the estimated PDF of all the data points in figure 18 for the different misregistration examples. As observed from figure 19, as the number of misregistered pixels increases, the SAL signal energy drops from a mean of 622 σ (0 misregistered pixels) to 476 σ (9 misregistered pixels). The clutter signal increases approximately 34 σ from 0 to 1 misregistered pixel, however, as the number of misregistered pixels continues to increase (up to 9), the clutter σ drops slowly from 60 σ to 51 σ, which, regardless, is far too low compared to the SAL signal energy level. As a result, no false alarms are detected.

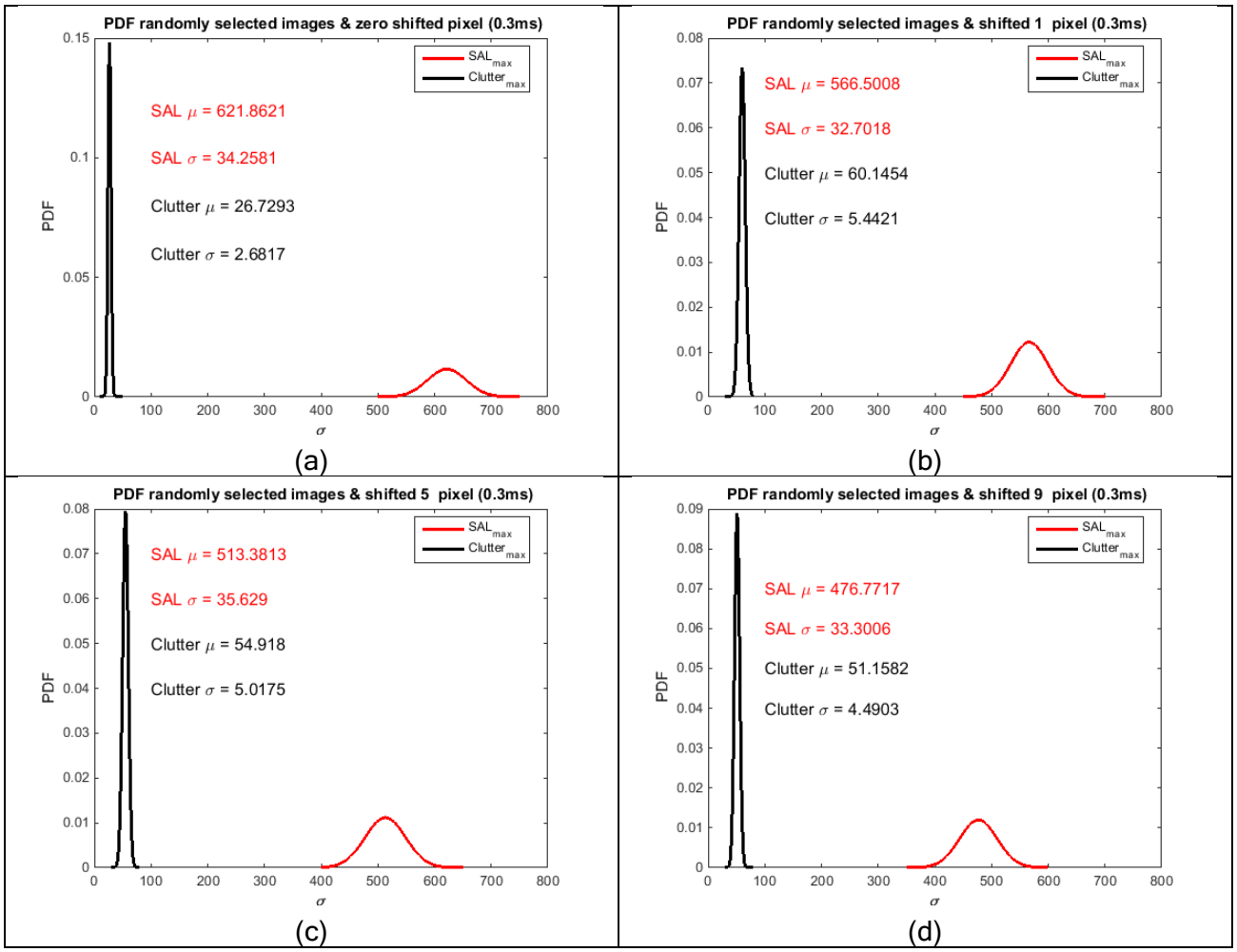

Note: As the number of misregistered pixels increases, the SAL signal strength decreases; however, the clutter energy is much lower than SAL energy, which allows us to detect the signal with no problem.

Figure 19
PDF of SAL and clutter for 0, 1, 5, and 9 misregistration pixels for 0.3-ms integration time

Thus, the effect on the clutter and SAL signal when decreasing the integration time by a factor of 10 is demonstrated. Decreasing the integration time shows that the shorter the integration time, the higher the SCR. For this case, even with 9 misregistered pixels, the SAL energy was much higher than the clutter.

Highpass Filter (900 nm) with 25-µs Integration Time

Next, a new highpass filter with a wider operating bandwidth is used. Widening the bandwidth implies (50 to 200 nm) that one is increasing the amount of clutter (spectrally) captured by the sensor. As a result, the integration time was decreased to 25 µs to reduce temporally the amount of clutter information captured with the sensor.

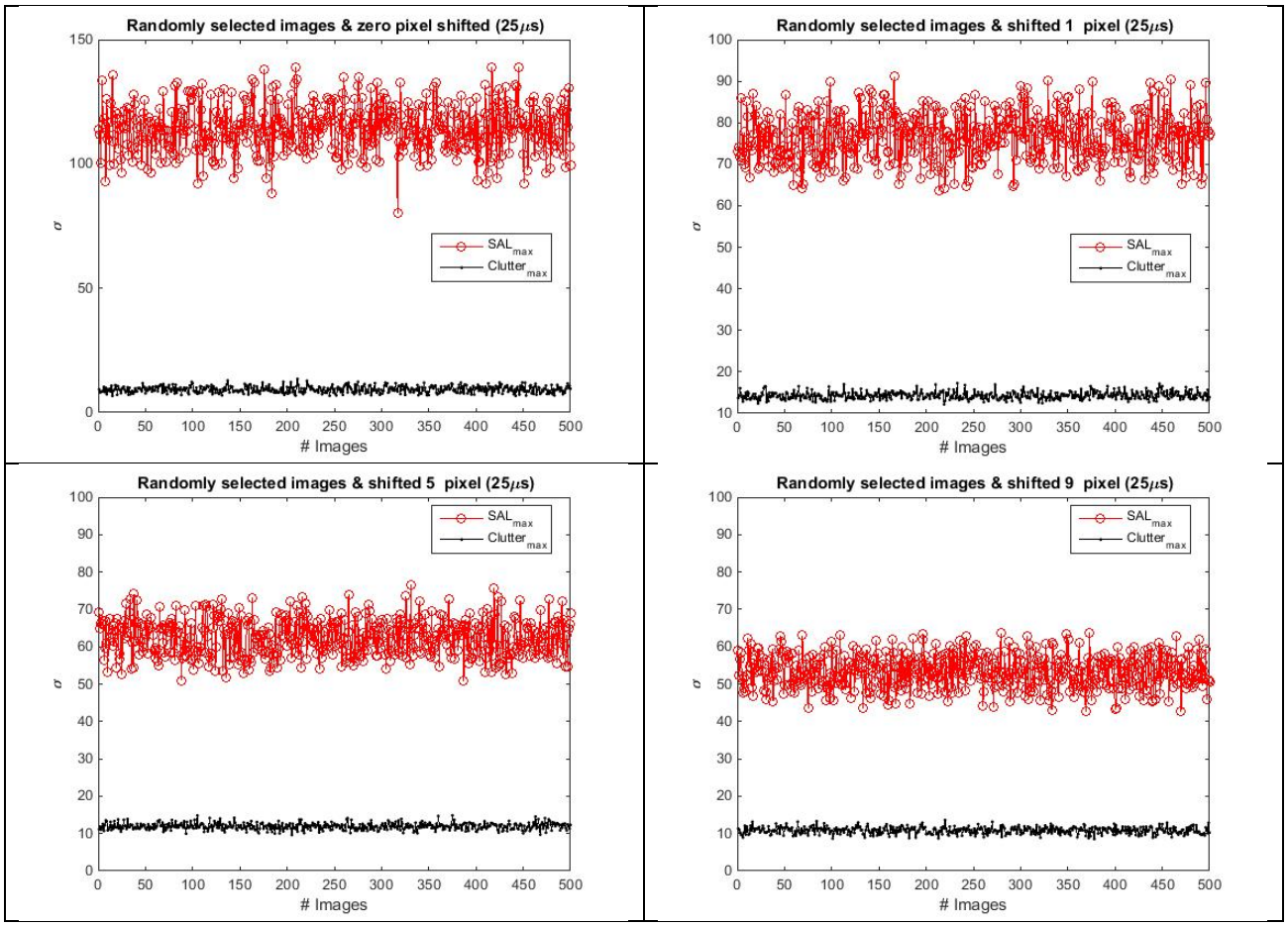

Note: The SAL signal energy is significantly greater than the clutter regardless of the number of misregistered pixels.

Figure 20
SAL and clutter energy comparison for 0, 1, 5, and 9 misregistered pixels for 25-μs integration time

Reducing the integration time with a wider operating bandwidth allowed the SAL signal strength in figure 20 to be above the clutter signal even with 9 misregistration pixels between the I_{SAL} and $I_{Clutter}$ imagery. From the image, there are no false positives for the 500 images that were processed for the different misregistration tests. The maximum SAL signal strength is always higher than maximum background clutter in all shifted pixels images. It should be noted that SAL signal also decreases in strength as the number of shifted pixels increases but SAL signal strength never approaches the clutter region, for example at 9 pixels shifted where clutter is below 20 σ, while the SAL signal is greater than 50 σ in terms of σ.

Figure 21 shows the PDF for the dataset shown in figure 20, which demonstrates that the highpass filter with 25-μs integration time allows the sensor to capture the SAL signal while reducing the amount of clutter information; and, as a result, by subtracting the SAL and clutter image, the residual image still shows a large enough difference between the SAL and residual clutter that no false alarms were detected.

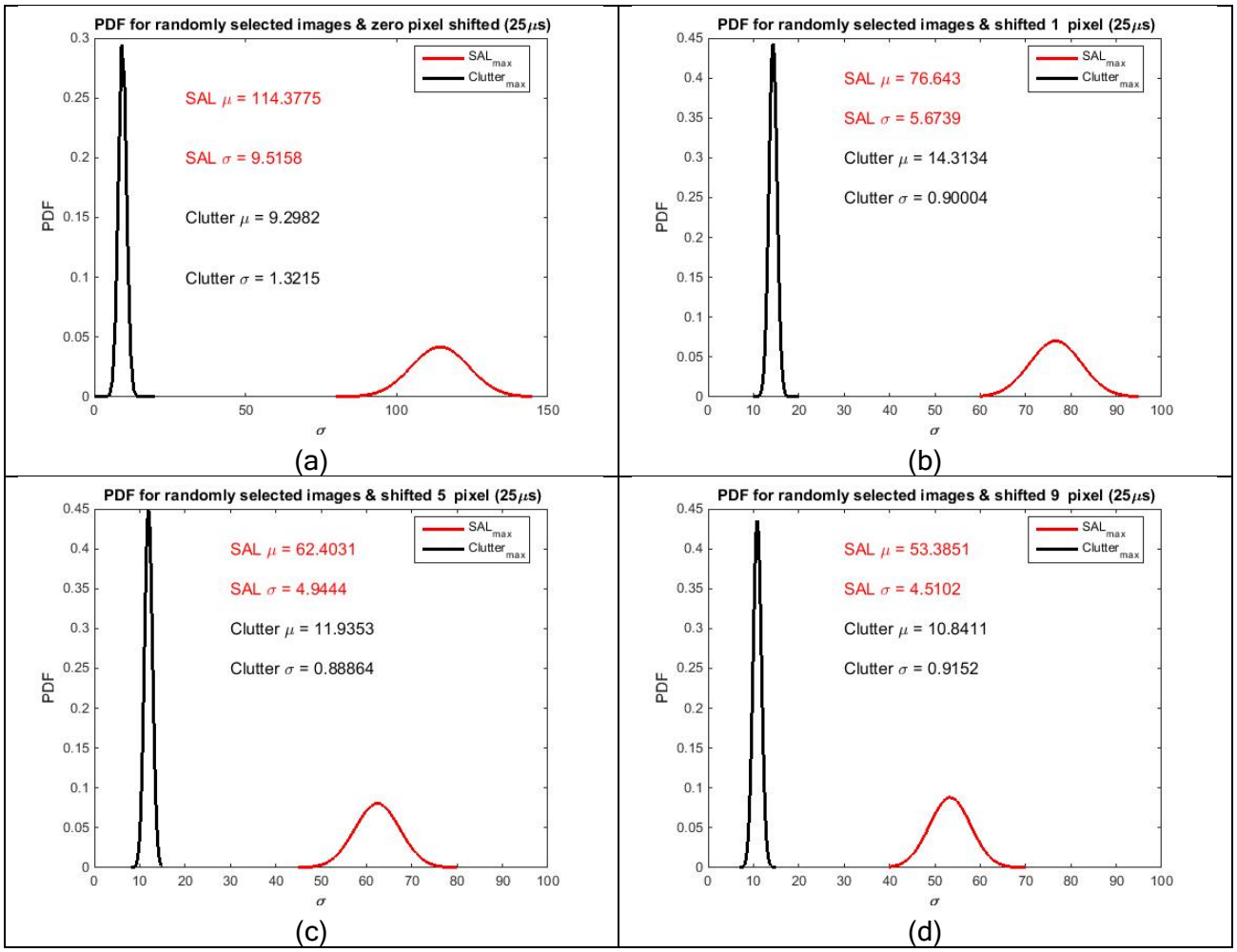

Figure 21
PDF of SAL and clutter for 0, 1, 5, and 9 misregistration pixels for 25-μs integration time

CONCLUSIONS

This report presented an analysis of how a CMOS sensor is able to detect a SAL signal in clutter. Furthermore, it was demonstrated how the choice of filter type and bandwidth as well as the sensor integration time both affect the system's ability to discriminate the SAL signal from possible false alarms. In this report, a false alarm was defined as any clutter pixel value that is close to or higher than the threshold; however, because a lot of clutter false alarms are randomly found in the picture from image to image, a threshold could be relaxed further. This portion of temporal false alarm tracking was not accomplished under this effort.

Furthermore, the effect of man-made lights and their effect in discriminating it from the SAL signal was explained, and the probability density function of SAL and clutter signals for all sets of imagery including images where the SAL and clutter imagery were purposedly misregistered was demonstrated. Lastly, it is proposed that one should use a narrow bandpass filter within the operating frequency of the laser with a very short integration time to provide high probability of discrimination between the SAL signal and background clutter.

REFERENCES

1. Robbins, M. S. and Weatherup, C., “A novel SAL detector giving enhanced spatial and temporal resolution,” Proc. SPIE 8020, Airborne Intelligence, Surveillance, Reconnaissance (ISR) Systems and Applications VIII, 802006; doi:10.1117/12.883823, 26 May 2011

2. Carlson, M., “Precision Guided Miniature Munitions,” 40th Annual Guns-Ammunition-Rockets-Missiles Conference, New Orleans, LA, 28 April 2005.

DISTRIBUTION LIST

U.S. Army CCDC AC
ATTN: FCDD-ACE-K
Picatinny Arsenal, NJ 07806-5000

Defense Technical Information Center (DTIC)
ATTN: Accessions Division
8725 John J. Kingman Road, Ste 0944
Fort Belvoir, VA 22060-6218

GIDEP Operations Center
P.O. Box 8000
Corona, CA 91718-8000
gidep@gidep.org

REVIEW AND APPROVAL OF ARDEC REPORTS

THIS IS A:

☒ **TECHNICAL REPORT** ☐ **SPECIAL REPORT**

☐ **MEMORANDUM REPORT** ☐ **ARMAMENT GRADUATE SCHOOL REPORT**

FUNDING SOURCE **WR.0029232.1.2.3**
[e.g., TEX3; 6.1 (ILIR, FTAS); 6.2; 6.3; PM funded EMD; PM funded Production/ESIP; Other (please identify)]

Analysis of Collected SAL (Semi-Active Laser) Images
Title

Affordable Precision Technology (APT)
Project

Zaw T. Han
João M. Romano
Luz Florez Manduca
Authors/Project Engineer

Report number/Date received (to be completed by LCSD)

973-724-5356 Extension | **B-407** Building | **RDAR-MEF-P** Author's Office Symbol

PART 1. **Must be signed before the report can be edited.**

a. The draft copy of this report has been reviewed for technical accuracy and is approved for editing.

b. Use Distribution Statement A X, B____, C____, D____, E____, or F____ for the reason checked on the continuation of this form. Reason: _____

1. If Statement A is selected, the report will be released to the National Technical Information Service (NTIS) for sale to the general public. Only unclassified reports whose distribution is not limited or controlled in any way are released to NTIS.

2. If Statement B, C, D, E, or F is selected, the report will be released to the Defense Technical Information Center (DTIC) which will limit distribution according to the conditions indicated in the statement.

c. The distribution list for this report has been reviewed for accuracy and completeness.

Jay W. Chang 7 Nov 17
Division Chief (Date)

PART 2. To be signed either when draft report is submitted or after review of reproduction copy.

This report is approved for publication.

Jay W. Chang 7 Nov 17
Division Chief (Date)

Arnold Klein 11/13/17
RDAR-CIS (Date)

LCSD 49 (1 Sept 16)
supersedes SMCAR Form 49, 20 Dec 06